PAPER • OPEN ACCESS

Overview of the recent experimental research on the J-TEXT tokamak

To cite this article: Y. Liang *et al* 2019 *Nucl. Fusion* **59** 112016

OPEN ACCESS
IOP Publishing | International Atomic Energy Agency
Nuclear Fusion
Nucl. Fusion **59** (2019) 112016 (13pp)
https://doi.org/10.1088/1741-4326/ab1a72

Overview of the recent experimental research on the J-TEXT tokamak

Y. Liang[1,2,3], N.C. Wang[1,a], Y.H. Ding[1], Z.Y. Chen[1], Z.P. Chen[1], Z.J. Yang[1], Q.M. Hu[4], Z.F. Cheng[1], L. Wang[1], Z.H. Jiang[1], B. Rao[1], Z. Huang[1], Y. Li[1], W. Yan[1], D. Li[1], H. Liu[5], L. Zeng[3], Y. Huang[1], D.W. Huang[1], Z.F. Lin[1], W. Zheng[1], F.R. Hu[1], K.J. Zhao[6], M. Jiang[7], Y.J. Shi[8], H. Zhou[1], S.T. Peng[1], W.X. Guo[1], L. Gao[1], Z.J. Wang[1], M. Zhang[1], K.X. Yu[1], X.W. Hu[1], Q. Yu[9], G. Zhuang[1,10], K.W. Gentle[11], Y. Pan[1] and the J-TEXT Team[b]

[1] International Joint Research Laboratory of Magnetic Confinement Fusion and Plasma Physics, State Key Laboratory of Advanced Electromagnetic Engineering and Technology, School of Electrical and Electronic Engineering, Huazhong University of Science and Technology, Wuhan 430074, People's Republic of China
[2] Forschungszentrum Jülich GmbH, Institut für Energie- und Klimaforschung—Plasmaphysik, 52425 Jülich, Germany
[3] Institute of Plasma Physics, Chinese Academy of Sciences, Hefei 230031, People's Republic of China
[4] Princeton Plasma Physics Laboratory, PO Box 451, Princeton, NJ 08543, United States of America
[5] Southwest Jiaotong University, Chengdu, People's Republic of China
[6] College of Nuclear Science and Engineer, East China University of Technology, PO Box 330013, Nanchang, People's Republic of China
[7] Southwestern Institute of Physics, Chengdu 610041, People's Republic of China
[8] Department of Nuclear Engineering, Seoul National University, Seoul, Korea, Republic of
[9] Max-Planck-Institut für Plasmaphysik, D-85748 Garching, Germany
[10] University of Science and Technology of China, Hefei 230026, People's Republic of China
[11] Institute of Fusion Studies, University of Texas, Austin, TX 78712, United States of America

E-mail: wangnc@hust.edu.cn

Received 19 November 2018, revised 3 April 2019
Accepted for publication 17 April 2019
Published 22 July 2019

Abstract

Recent J-TEXT research has highlighted the significance of the role that non-axisymmetric magnetic perturbations, so called three-dimensional (3D) magnetic perturbation (MP) fields, play in a fundamentally 2D concept, i.e. tokamaks. This paper presents the J-TEXT results achieved over the last two years, especially on the impacts of 3D MP fields on magnetohydrodynamic instabilities, plasma disruptions and plasma turbulence transport.

On J-TEXT, the resonant MP (RMP) system, capable of providing either a static or a high frequency (up to 8 kHz) rotating RMP field, has been upgraded by adding a new set of 12 in-vessel saddle coils. The shattered pellet injection system was built in J-TEXT in the spring of 2018. The new capabilities advance J-TEXT to be at the forefront of international magnetic fusion facilities, allowing flexible study of 3D effects and disruption mitigation in a tokamak.

[a] Author to whom any correspondence should be addressed.
[b] See appendix.

The fast rotating RMP field has been successfully applied for avoidance of mode locking and the prevention of plasma disruption. A new control strategy, which applies pulsed RMP to the tearing mode only during the accelerating phase region, was proved by nonlinear numerical modelling to be efficient in accelerating mode rotation and even completely suppresses the mode. Remarkably, the rotating tearing mode was completely suppressed by the electrode biasing. The impacts of 3D magnetic topology on the turbulence has been investigated on J-TEXT. It is found that the fluctuations of electron density, electron temperature and plasma potential can be significantly modulated by the island structure, and a larger fluctuation level appears at the X-point of islands. The suppression of runaway electrons during disruptions is essential to the operation of ITER, and it has been reached by utilizing the 3D magnetic perturbations on J-TEXT. This may provide an alternative mechanism of runaway suppression for large-scale tokamaks and ITER.

Keywords: tokamak, resonant magnetic perturbations, disruption, turbulence, magnetic island, tearing mode control, runaway current

(Some figures may appear in colour only in the online journal)

1. Introduction

As part of a long-term research program, the Joint-TEXT (J-TEXT) [1–5] experiments aim to develop fundamental physics and control mechanisms of high temperature tokamak plasma confinement and stability in support of successful operation of ITER [6] and the design of the future Chinese fusion reactor, CFETR [7]. Recent research has highlighted the significance of the role that non-axisymmetric magnetic perturbations (MPs), so called three-dimensional (3D) MP fields, play in a fundamentally 2D concept, i.e. tokamaks.

The J-TEXT tokamak is a conventional iron core tokamak, operated at a major radius $R_0 = 1.05$ m, minor radius $a = 25$–29 cm with a movable titanium-carbide-coated graphite limiter. The typical J-TEXT discharge in the limiter configuration is done with a toroidal field B_t of ~2.0 T, a plasma current I_p of ~200 kA, a pulse length of 800 ms, plasma densities n_e of 1–7 $\times$ 10^{19} m^{-3}, and an electron temperature T_e of ~1 keV. On J-TEXT, 3D MP fields can be induced by either the application of resonant MPs (RMPs) or the appearance of core magnetohydrodynamic (MHD) modes. In this paper, the J-TEXT results achieved over the last two years, especially on the impacts of 3D MP fields on MHD instabilities, plasma disruptions and plasma turbulence transport will be presented.

2. Progress of the auxiliary systems

In the past two years, there was major progress in the two auxiliary systems, i.e. the RMP system [8, 9] and the shattered pellet injection (SPI) system [10].

In the spring of 2017, the RMP system was upgraded by adding a new set of 12 in-vessel saddle coils (3 rows $\times$ 4 columns $\times$ 2 turns), and the total number of in-vessel RMP coils increased from 12 to 24 (3 rows $\times$ 8 columns), as shown in figure 1. To date, this RMP system has unique capabilities to provide not only high frequency (up to 8 kHz) ac non-axisymmetric MPs, but also is more capable and flexible when adjusting its amplitude (up to 3.5 mT of $m/n = 2/1$ RMP) and spectrum (the n up to 4), where m and n are the poloidal and toroidal mode number. These new capabilities advance J-TEXT to being at the forefront of international magnetic fusion facilities, allowing for the flexible study of 3D effects in a tokamak.

In the spring of 2018, the SPI system [10] was built in J-TEXT. Figure 2 displays the schematic drawing of the whole SPI system, which is about 3.5 m long. A pellet is formed with 5 mm diameter and 1.5–10 mm length at a temperature of 64 K. The pellet is formed with argon and the amount of injected argon particles is from 0.7 $\times$ 10^{20} to 5.0 $\times$ 10^{21} atoms. Helium gas or argon gas, as the propellant gas for the pellet, accelerates it to 150–300 m s^{-1} with a pressure of 0–20 bar (the max is 80 bar). The pellet will be shattered before entering the plasma by impacting on a strike plate situated at the entrance to the tokamak vacuum chamber. The shattered pellets enter the plasma within 30 ms from the command sent by the central control system. The time interval between injection cycles is about 8 min.

3. Control of tearing modes (TMs)

TMs, especially the $m/n = 2/1$ TM, deteriorate the confinement performance significantly [11]. In addition, the TM could be decelerated to a non-rotating state, leading to the so called locked mode (LM). The LM usually grows to a very large amplitude, and it is one of the most common causes of major disruption in a tokamak [12, 13]. Therefore, active control of the TM is an important issue for future fusion reactors, e.g. ITER and CFETR.

Previous experimental and theoretical studies showed that the RMP influences both the rotation and the width of the TM [14–16], accelerating (decelerating) the TM when $\pi < \xi < 2\pi$ ($0 < \xi < \pi$) and stabilizing (destabilizing) the TM when $0.5\pi < \xi < 1.5\pi$ ($-0.5\pi < \xi < 0.5\pi$), where ξ is the phase difference between the RMP and the TM. As a result, the static RMP could apply a net stabilizing and braking effect on a rotating TM. This section briefly summarizes the recent studies on TM control by applying rotating or modulated

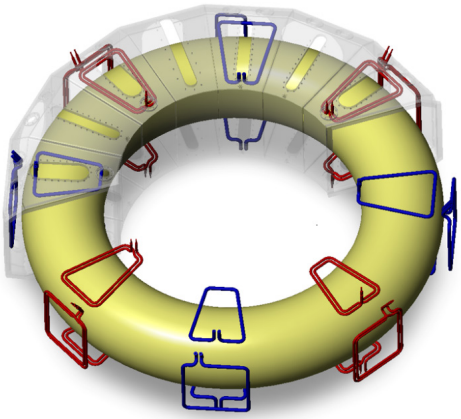

Figure 1. The in-vessel RMP coils on J-TEXT, consisting of 12 single-turn coils (blue) [8] and 12 double-turn coils (red) [9].

RMP field and by biased electrode, while a detailed description is presented in [17].

3.1. Control of the TM rotation by applying a rotating RMP field

The electromagnetic (EM) torque applied by RMP on the TMs can be used as an effective tool to control the rotation of TMs and the background plasmas. The application of a static RMP field always leads to the deceleration and locking of rotating TMs, followed by a major disruption [14, 18]. By applying a RMP field rotating faster than the TM, the rotation acceleration of a TM in J-TEXT was first observed in 2013 [19]. It is shown later that the TM could either be accelerated or decelerated, if the initial slip frequency $f_s = f_{TM} - f_{RMP}$ is negative or positive [20]. Meanwhile, the particle confinement is improved if the TM is accelerated, which is in contrast to the density decrease for TM-locked to static RMP [21].

Recently, the plasma rotations were measured by the spectrometers both in the edge ($r/a = 0.6$–0.9) for CV (C^{4+}) [22] and in the core ($r/a < 0.4$) for helium-like argon (Ar^{16+}) [23, 24], during the application of the rotating RMP (RRMP). By locking the TMs to the RRMP, the toroidal rotations of the impurities were also accelerated or decelerated depending on the sign of f_s [25], as shown in figure 3. With the modification of high frequency power supplies, the change of the RMP frequency within one discharge was achieved [26]. As shown in figure 4, the frequency of the RMP was reduced by ~1 kHz within 1 ms at 0.321 s and 0.371 s. The frequency of the TM is also reduced after a short time lag, which is needed for the locking of TM to the RRMP.

According to the observation in [19], the TM could be suppressed by maintaining the frequency of RRMP slightly higher than that of the TM, so that the RRMP could apply a net stabilizing effect on TM without locking. Preliminary studies show that the frequency response of this hopping-frequency PS is not fast enough to avoid mode locking and to keep a small f_s. A new power supply (PS), which is capable of varying frequency continuously, has been built [27] and will be applied for this control strategy in the following campaign.

3.2. Control of the locked modes by applying a rotating RMP field

The capacity of the RRMP in accelerating TMs can also be used to control the LMs. The RMP, rotating at a few kilohertz, was applied and unlocked the TMs successfully in J-TEXT [28]. It is found that the unlocking threshold of RRMP is smaller at a lower static error field or lower RRMP frequency. Further analysis reveals that the phase of the LM is forced to oscillate by the EM torque applied by RRMP [29] and that the LM is unlocked with a large amplitude of the phase oscillation. To set-up reproducible LMs, these discharges were carried out with non-disruptive LMs which were maintained by a small static RMP.

Recently the disruptive discharges induced by the intrinsic mode locking were performed by increasing the plasma current and hence reducing the edge safety factor from 3 towards 2, as shown by discharge #1052960 in figure 5. The braking of the TM lasted for ~5 ms and the disruption followed about ~10 ms after the mode locked. The RRMP applied after the mode locked was not strong enough to unlock the LM, hence the disruption occurred. Trigged by the mode locking warning system, the 3 kHz RRMP was applied before the mode locked in discharge #1052963 (blue lines in figure 5). The TM was accelerated to 3 kHz and the intrinsic mode locking was avoided. As a result, the disruption was prevented [17].

3.3. Suppressing magnetic island and accelerating its rotation by modulated RMP

The above control strategy applies a rigid rotating RMP field, hence the TM undergoes acceleration/deceleration or stabilizing/de-stabilizing effects successively within a TM rotation period in the RRMP rest frame. To enhance the *good* effect (also to reduce the *bad* effect) of RMP on the TM, a new control is proposed to apply pulsed RMP to the TM only during the accelerating phase region, i.e. within $\pi \leqslant \xi \leqslant 2\pi$, or during the accelerating and stabilizing phase region, i.e. within $\pi \leqslant \xi \leqslant 1.5\pi$ [30]. By nonlinear numerical modelling, it was proved to be efficient in accelerating the mode rotation and even completely suppresses the mode, as shown in figure 6.

A dedicated pulsed PS [31] and the corresponding real time control system [32] with the measurement of island locations [33] have been built on J-TEXT. The first experimental attempt with the pulsed RMP has demonstrated the acceleration effect with a relative low amplitude of RMP [32]. The TM frequency could be increased by ~0.3 kHz with 1 kA of RMP coil current. A new pulsed PS [27], with a maximum current of 3 kA, has been built to further testify the impact of pulsed RMP on the frequency and width of the TMs. The preliminary experiment shows that the TM could be accelerated from 4.5 kHz to 7 kHz [17]. Further commissioning will allow higher operation frequency of this PS, and perhaps lead to further rotation acceleration of TMs.

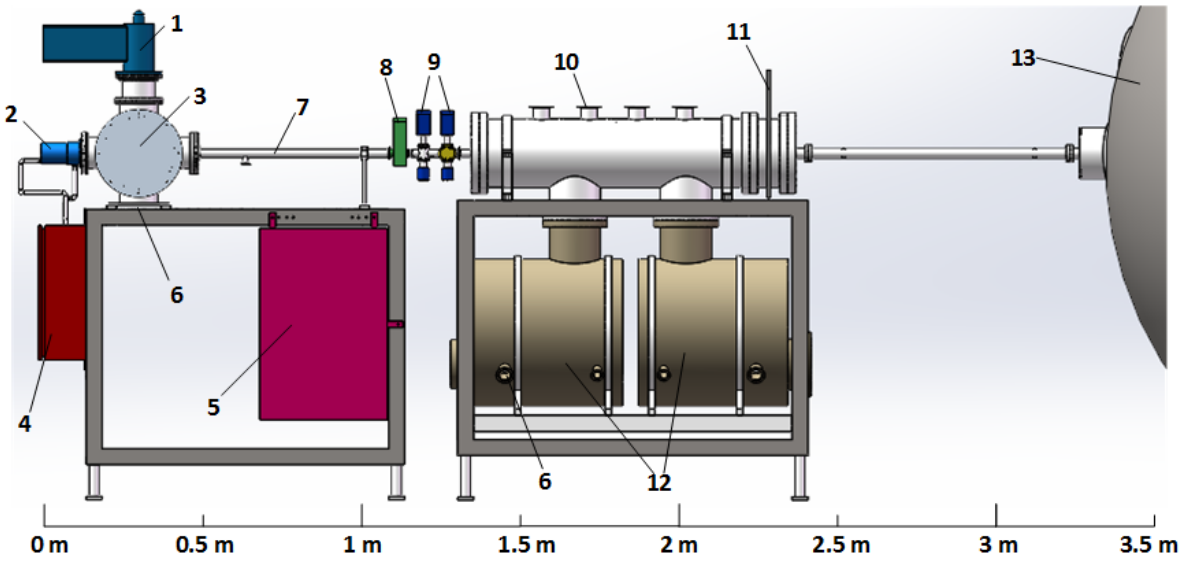

Figure 2. The 3D layout diagram of the SPI system for the J-TEXT tokamak: 1—cryocooler, 2—pellet acceleration system, 3—pellet injector, 4—gas tube system, 5—electrical system, 6—pump flange, 7—guide tube, 8—gate valve, 9—measurement system, 10—high and low vacuum sensors, 11—vacuum gate valve, 12—buffer chamber, 13—J-TEXT tokamak. Reprinted from [10], with the permission of AIP Publishing.

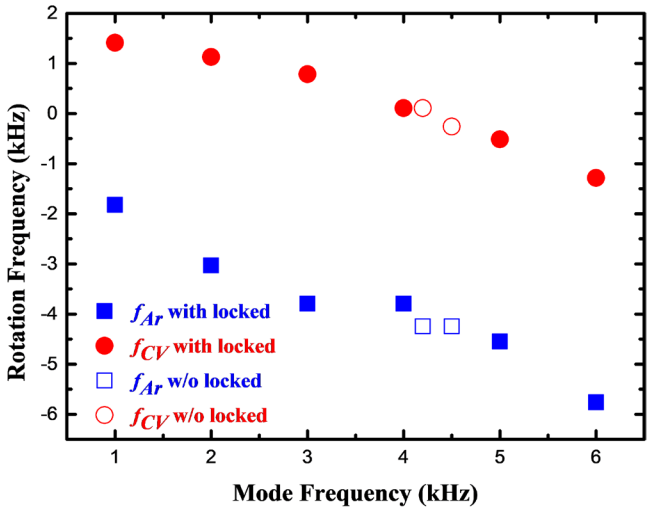

Figure 3. The dependence of the toroidal rotation frequency of the impurities in the core, f_{Ar}, and edge, f_{CV}, on the tearing mode frequency with (open) and without (filled) rotating RMP. Reproduced from [25]. © IOP Publishing Ltd. All rights reserved.

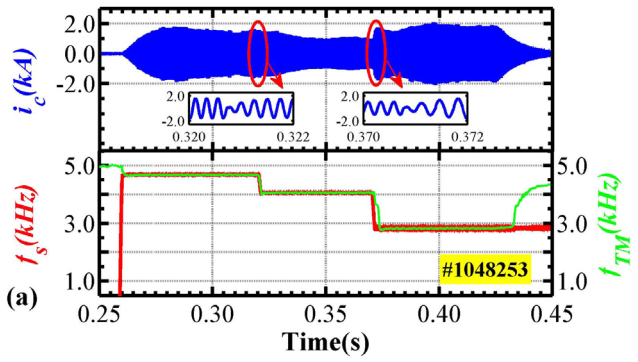

Figure 4. Control of the TM frequency within one discharge by applying RRMP with varying frequency. (Top) RMP coil current; (bottom) the frequency of RMP field (red) and TM (green) Reproduced from [26]. © 2018 Hefei Institutes of Physical Science, Chinese Academy of Sciences and IOP Publishing. All rights reserved.

3.4. Control of the TM by a biased electrode

The biased electrode is an efficient method to change the plasma parameters and flows. An electrode was inserted 2 cm inside the plasmas, while the $q = 2$ surface was at about $r \sim 19$ cm, i.e. 4.5 cm inside the electrode location. The electrode was biased either positively or negatively to investigate its impact on the TM in J-TEXT [34]. It is found that for a negative bias voltage, the TM amplitude is reduced, and the mode frequency is increased accompanied by the increased toroidal plasma rotation speed in the counter-I_{p} direction. For a positive bias voltage, the mode frequency is decreased together with the change of the rotation velocity towards the co-I_{p} direction, and the mode amplitude is increased. Figure 7 displays the statistic results that the variations in the toroidal rotation speed, ΔV_{ϕ}, the 2/1 mode frequency, f_{MHD}, and its amplitude, $\delta B_{\theta,\mathrm{nor}}$, depend linearly on the bias voltage, U_{EB}.

Remarkably, the TMs were completely suppressed [34] by the negative biasing with a threshold voltage of -300 V at $q_{\mathrm{a}} = 3$, while the TMs were locked if the positive biasing was above 100 V. The experimental results suggest that applied electrode biasing is a possible method for the avoidance of mode locking and disruption, which will be investigated in the future.

4. Progress on the disruption mitigation

The disruption-generated high energy runaway electrons (REs) which are a great threat to the safe operation of a fusion reactor [11, 35–37]. It is of great importance to understand the mechanisms responsible for RE generation, the confinement of REs, and to find reliable methods to control or suppress the REs. In this section, we summarize the recent J-TEXT studies on the RE generation [38, 39] and the RE suppression by actively driven

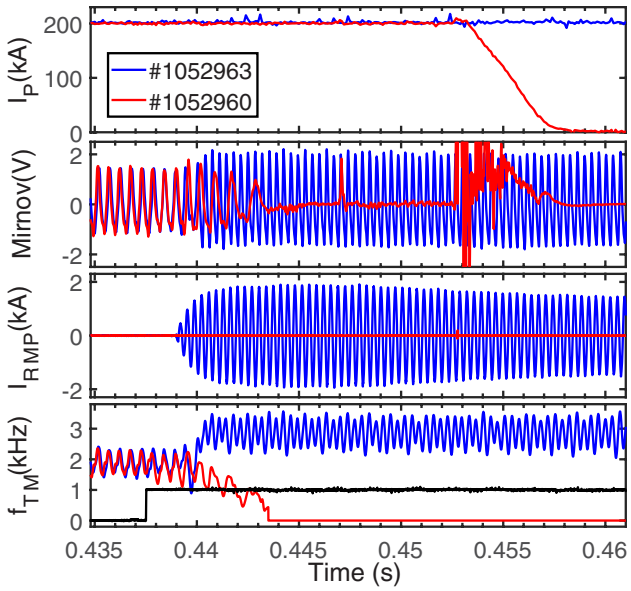

Figure 5. Disruption avoidance by the feedback application of RRMP. (Red) without RRMP; (blue) RRMP applied by feedback control [17].

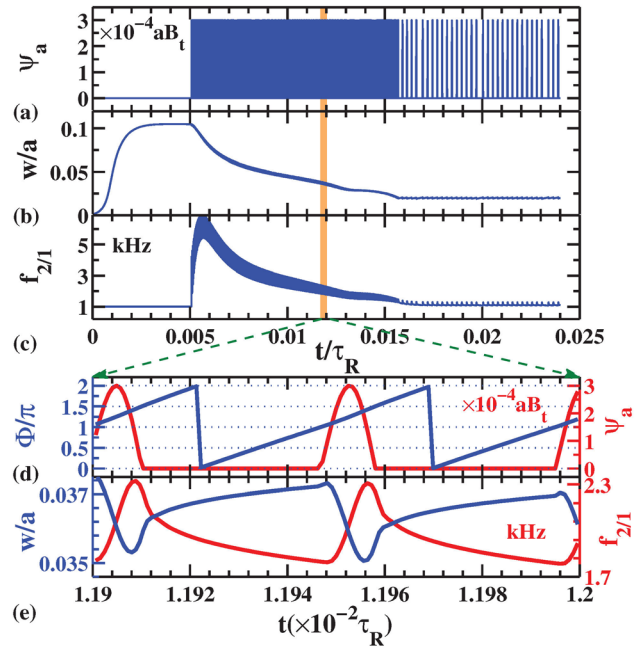

Figure 6. Complete suppression of a TM and accelerating its rotation by applying a modulated RMP in the acceleration and stabilizing phase region, (π, 1.5π). Reproduced courtesy of IAEA. Figure from [30]. Copyright 2016 IAEA.

magnetic perturbations [40–43] in the disruptions triggered by the massive gas injection (MGI). The first result on the disruption mitigation by using the SPI system is also presented [10].

4.1. Runaway electron generation during MGI triggered disruptions

A systematic study of disruption-generated REs has been performed in J-TEXT [38]. During the intended disruption by MGI of argon in J-TEXT, the RE plateau is more easily

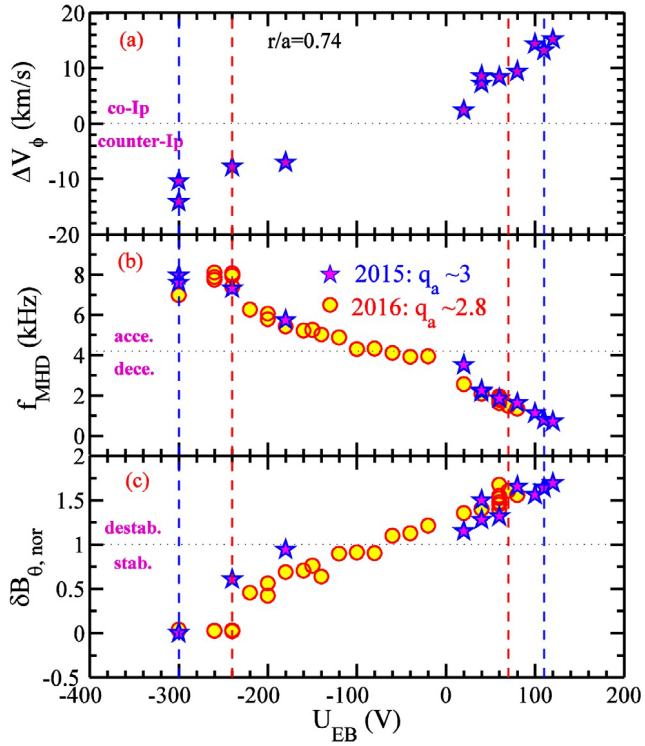

Figure 7. The statistical results of (*a*) the variation of rotation at $r/a = 0.74$, (*b*) TM frequency f_{MHD} and (*c*) normalized poloidal magnetic perturbation $\delta B_{\theta,nor}$ versus bias voltage. $\delta B_{\theta,nor} = \delta B_\theta/\delta B_{\theta 0}$, $\delta B_{\theta 0}$ and δB_θ are the initial and steady amplitude of δB_θ before and during the application of EB, respectively. Reproduced courtesy of IAEA. Figure from [34]. Copyright 2017 IAEA.

obtained with a higher loop voltage and shorter onset time of high loop voltage. Magnetic fluctuations are observed at the beginning of the current quench (CQ) during the disruptions. RE currents are only obtained in the region of low electron density and low magnetic fluctuation, similar as the previous observation on TEXTOR [44]. Figure 8 displays I_{RE}/I_P as a function of the maximum magnetic fluctuation amplitude during the CQ, $\delta B/B_t$, and the electron density, n_e, before the disruptions. In J-TEXT the RE plateau is not visible unless the product of $\delta B/B_t$ and the square of n_e is lower than a threshold. For shots with lower product than the threshold it is found that I_{RE}/I_P decrease with the product for a wide range of B_t and I_p.

Experimental evidence supporting that the theory of hot tail RE generation [45] might be playing a role has also been found. With higher temperature before the disruption, more RE seeds are generated via the hot tail mechanism during the thermal quench. By increasing the electron temperature, an obvious RE plateau is observed even with a low toroidal magnetic field (1.2 T), since the hot tail RE generation [46] is enhanced so much at higher T_e that the total RE generation exceeds the enhanced RE losses at lower B_t [44].

4.2. MHD activities and the cooling process during MGI triggered disruptions

In the disruption mitigation by injecting impurities, the deposition of impurities at the center of the plasma is the key for the radiation of plasma energy and runaway suppression.

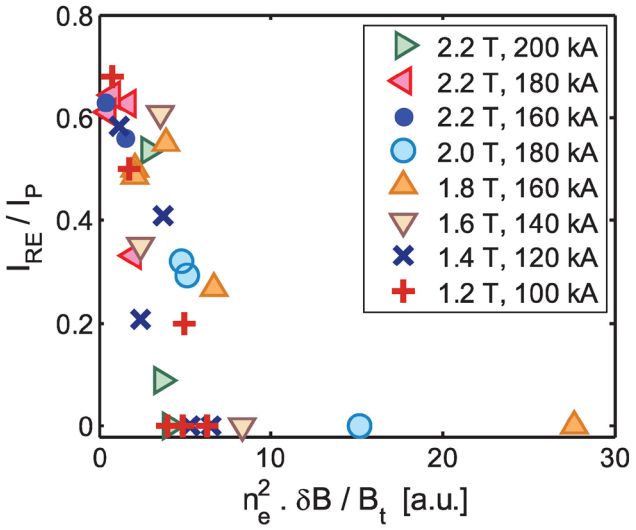

Figure 8. I_{RE}/I_P in J-TEXT disruptions as function of normalized magnetic fluctuation level and pre-disruption electron density. Reproduced courtesy of IAEA. Figure from [38]. Copyright 2017 IAEA.

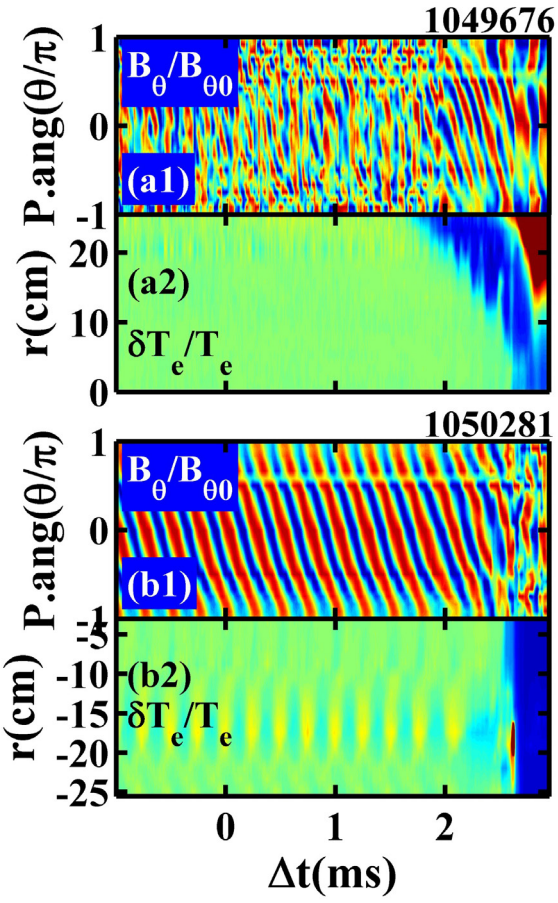

Figure 9. The time evolution of MHD instability and thermal quench due to MGI, without (#1049676) and with (#1050281) a pre-existing 2/1 TM. Reproduced from [47]. © 2018 IAEA, Vienna. CC BY 3.0.

Recent J-TEXT experiments show that the injection of a massive amount of argon can cool the plasma from edge to core region, and the cooling process is accompanied by different MHD modes when the gas jet reaches the corresponding

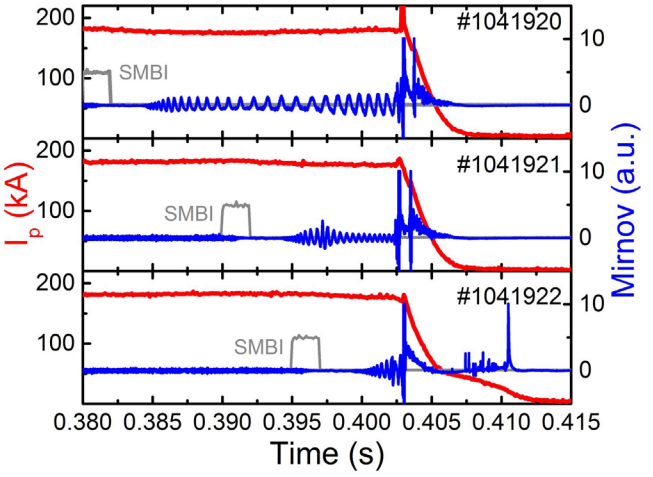

Figure 10. The REs generation impacted by the SMBI at different times, which led to different mode amplitudes. Reproduced from [43]. © IOP Publishing Ltd. All rights reserved.

rational surfaces [47]. After the argon atoms are injected, a high-m MHD mode is initiated. As the impurity cools the plasma deeper, the MHD mode changes to a lower-m mode until a 2/1 mode is initiated and a thermal quench (TQ) started.

A pre-existing large 2/1 TM can significantly increase the penetration speed of a gas jet across the rational surfaces as shown in figure 9. The cooling process lasted ~1.4 ms in #1049676, where no large TM existed before MGI. With the pre-existing large TM in #1050281, the cooling from the edge to the core occurred at the same time. These results indicate that the 2/1 mode plays an important role in the penetration process. It will be shown in section 4.3 that the actively triggered magnetic island could assist the suppression of the RE currents.

4.3. Suppression of REs by RMP and SMBI

The RE confinement can be influenced by the magnetic topology change from the nested flux surfaces, hence the RE generation can be significantly impacted. In J-TEXT, the formation of magnetic island or even stochastic layer can be actively driven by applying either supersonic molecular beam injection (SMBI) [43] or RMP fields [40–42] before the MGI triggered disruption occurs, and the RE can be suppressed.

The SMBI excites magnetic islands, as long as the injected hydrogen quantity is above a certain threshold in J-TEXT [48]. Moreover, the RE loss increased rapidly if large TMs were excited [43]. By applying SMBI to induce TMs with sufficient amplitude, the generation of REs can be completely suppressed during the MGI triggered disruptions, as shown by discharges #1041920 and #1041921 in figure 10. The growth of 2/1 TM induced by SMBI is followed by MHD oscillations measured by ECE channels at the TM frequency even inside the $q = 1$ rational surface, which replaced the regular sawtooth crashes. The details can be found in figure 10 in [43]. The later injection of SMBI in #1041922 led to a smaller mode amplitude, which did not have enough time to grow to a sufficient amplitude before MGI triggered. The regular sawtooth crashes remained, the intact magnetic surface may still exist outside the $q = 1$ surface and would confine the REs

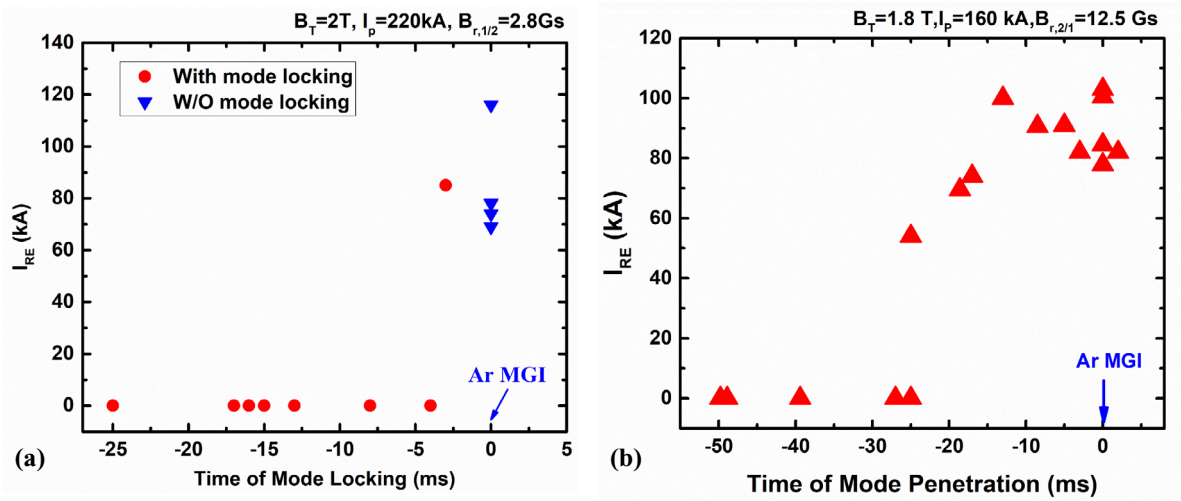

Figure 11. Dependence of the runaway current on the time of (*a*) mode locking and (*b*) mode penetration before the disruptions. The Ar MGI trigger time corresponds to $t = 0$ s. (*a*) Reproduced from [41]. © 2018 IAEA, Vienna. CC BY 3.0. (*b*) Adapted from [42]. © IOP Publishing Ltd. All rights reserved.

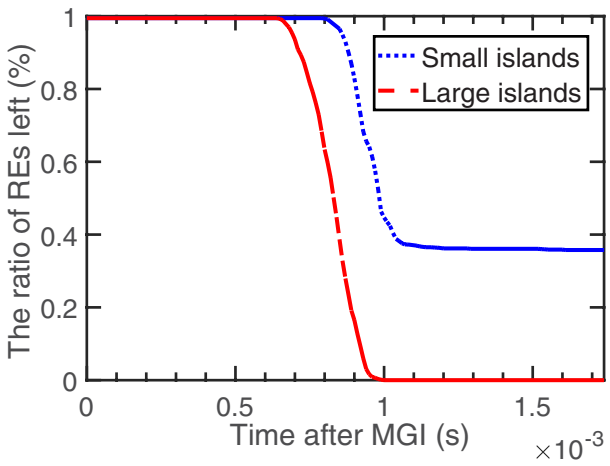

Figure 12. The ratio of REs left during disruptions by NIMROD simulation. About 920 REs with 150 keV kinetic energy are randomly distributed on the area of a poloidal cross section at a certain toroidal angle. Reproduced from [42]. © IOP Publishing Ltd. All rights reserved.

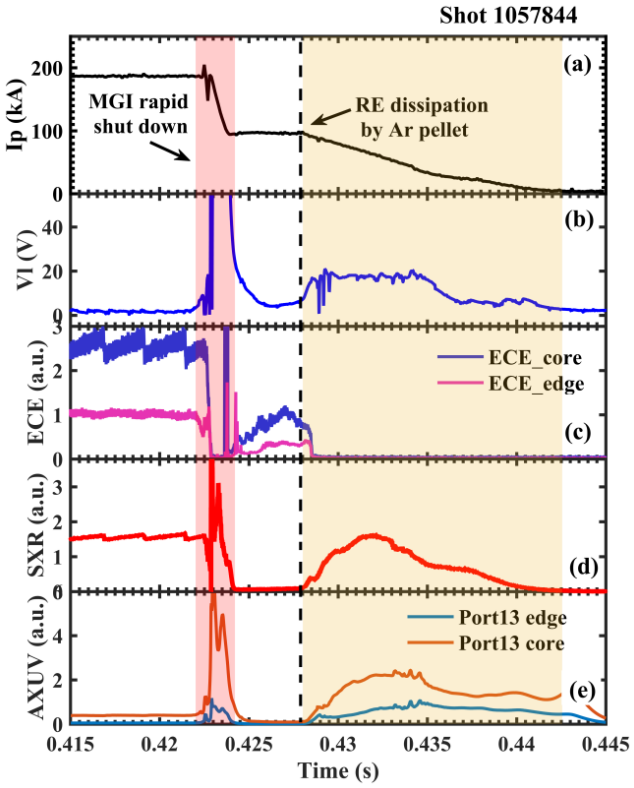

Figure 13. The runaway current dissipation with SPI in J-TEXT. The MGI was applied to induce the RE plateau before MGI. Reprinted from [10], with the permission of AIP Publishing.

generated during disruption [49]. The RE was only partially suppressed in #1041922. Applying hydrogen SMBI at the same time with argon MGI also demonstrates a complete suppression of the RE current generation.

A large 2/1 locked island can be formed due to the locking of a pre-existing rotating island or the RMP penetration. The RE generation can be completely suppressed, if the locked island is formed with enough time ahead of the MGI [41, 42], named as critical lead time, as shown in figure 11. It is found that the critical lead time of RE suppression is longer for RMP penetration than that for mode locking. This is related to the fact that the width of the locked island grows faster in the case of mode locking than that of RMP penetration. Note that this observation does not have to contradict the previous observation, where the RE production was enhanced by RMP [40]. In the previous case, the RMP amplitude was so low that no locked mode was excited before the MGI. Recent experimental results show that the RE generation decreased again at higher RMP amplitude due to the RMP penetration.

The NIMROD simulation has also demonstrated that the large magnetic islands have the ability to enhance the REs seed loss during disruptions. The simulation result of the ratio of the REs left during disruptions is illustrated in figure 12. The REs are lost quickly in the case of larger islands than the case of small islands during disruption. These results suggest

that the magnetic perturbation can act as an alternative way to mitigate runaway electrons in tokamak disruptions.

4.4. First result on the disruption mitigation by the SPI system

Figure 13 displays a successful dissipation of the MGI-induced runaway current by SPI [10], with $I_p = 180$ kA, $n_e = 1.5 \times 10^{19}$ m^{-3}, $B_t = 2.2$ T and $q_a = 3.6$. Following the triggering of the MGI valve at 0.42 s, about 5×10^{19} argon atoms were injected into the plasma and cooled the plasma from 0.422 s to 0.423 s. The CQ happened at 0.423 s following induction of a large loop voltage. Then, a runaway current plateau about 100 kA was formed at 0.424 s. The increase of the electron cyclotron emission (ECE) signal was caused by the generation of non-thermal electrons during the runaway current plateau. The typical RE beam on J-TEXT lasts for around 10 ms, which is much shorter than that needed for shatter pellets entering plasma from the SPI trigger. So the argon pellet with 4.5 mm length, 5 mm diameter was injected with a speed of 250 m s^{-1} in advance, i.e. at 0.405 s. The shattered pellets reached the plasma after 23 ms, i.e. 5 ms after the formation of RE beam. Then the pellets started to dissipate the runaway beam, while the radiation measured by soft x-ray (SXR) and AXUV signals started to increase. The argon SPI dissipated the runaway current at a rate of approximately 12 MA s^{-1}.

4.5. Disruption prediction and avoidance

To achieve the successful mitigation of disruption, a reliable disruption prediction is needed with sufficient warning time. In the previous works on J-TEXT, two predictors based on neural networks were developed to predict the locked mode disruption [50] and density limit disruption [51]. The previous networks were trained and tested by off-line data. Recently, an on-line density limit disruption prediction and the avoidance system based on a neural network has been built on J-TEXT [52]. The neural network has been improved from a simple multi-layer design to a hybrid two-stage structure. The first stage is a custom network which uses time series diagnostics as inputs to predict plasma density, and the second stage is a three-layer feedforward neural network to predict the probability of density limit disruptions. It can predict the plasma density as well as the density limit disruption. It is found that hybrid neural network structure, combined with radiation profile information as input can significantly improve the prediction performance, especially the average warning time (T_{warn}). In particular, T_{warn} is eight times better than that in previous work [51] (from 5 ms to 40 ms). In off-line tests, the system can achieve a performance of successful alarm rate >90%, false alarm rate <10% and average warning time >30 ms in a specific threshold range. The on-line density limit disruption avoidance system consists of an on-line density limit disruption predictor, by implementing the hybrid neural network on LabVIEW-RT platform, and a plasma density feedback control system based on the POLARIS [53]. This system can predict the plasma density as well as a density limit disruption, as shown by a density ramp-up discharge in figure 14. The

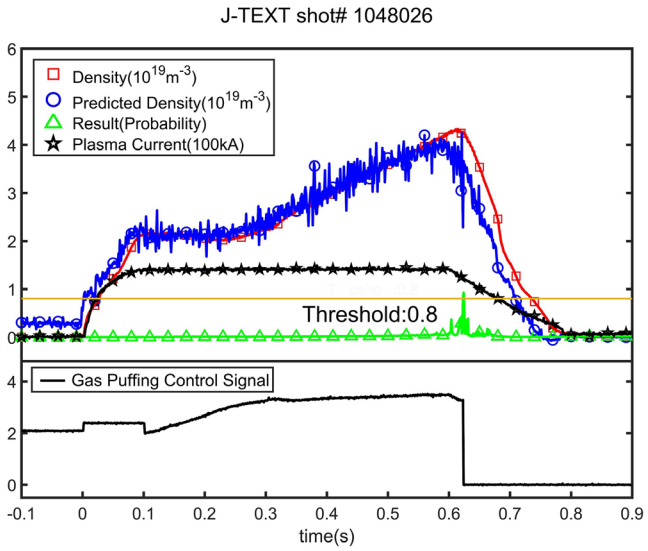

Figure 14. A density ramp-up discharge with on-line density limit disruption prediction and the disruption avoidance system. The disruption was avoided by closing the GPC valve immediately at 0.61 s when a disruption was predicted. Reproduced courtesy of IAEA. Figure from [52]. Copyright 2018 IAEA.

density limit disruption is successfully avoided by closing the gas puffing control (GPC) valve immediately when the disruption is predicted (figure 14). These results demonstrate the successful prediction and avoidance of density limit disruption on J-TEXT.

5. Turbulence and transport study

The impacts of 3D magnetic topology on the turbulences, and interplay between the turbulence and plasma rotation have been investigated on J-TEXT. It is found that the fluctuations of plasma potential [54], electron density [55] and electron temperature [56] can be significantly modulated by the island structure, and a larger fluctuation level appears at the X-point of island. By applying SMBI, the multi-channel non-local transport (electron temperature, particle, and momentum), possibly due to turbulence spreading, has been observed for the first time on J-TEXT [57]. For understanding the physics of intrinsic rotation, a new mechanism named turbulent acceleration has been developed [58–61].

5.1. Impact of magnetic island on the turbulence

The temporal-spatial structures of turbulence and plasma flows near the 3/1 magnetic islands are investigated by using Langmuir probe arrays and Mirnov coils in the edge plasmas of J-TEXT tokamak. The long-range correlation analysis is utilized. The structures of the flows are similar to those observed in the magnetic islands as $m/n = 3/1$. At the $q = 3$ surface, the reversal of the potential fluctuations for the flows is observed and the reduction of the powers is pronounced. Figures 15(*a*) and (*b*) show the spatial-temporal distributions of the potential fluctuations and the turbulence envelopes, respectively. Here, the dashed curves indicate the magnetic islands. The reversal

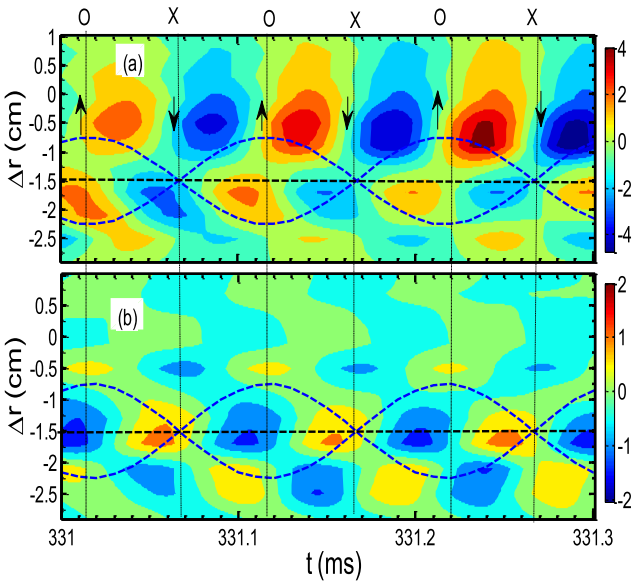

Figure 15. The contours of $m/n = 3/1$ potential fluctuations (a) and turbulence envelope in the island frequency bands (b), with volt the unit of the color bar. The magnetic islands are indicated by the dashed curves. Reproduced courtesy of IAEA. Figure from [54]. Copyright 2017 IAEA.

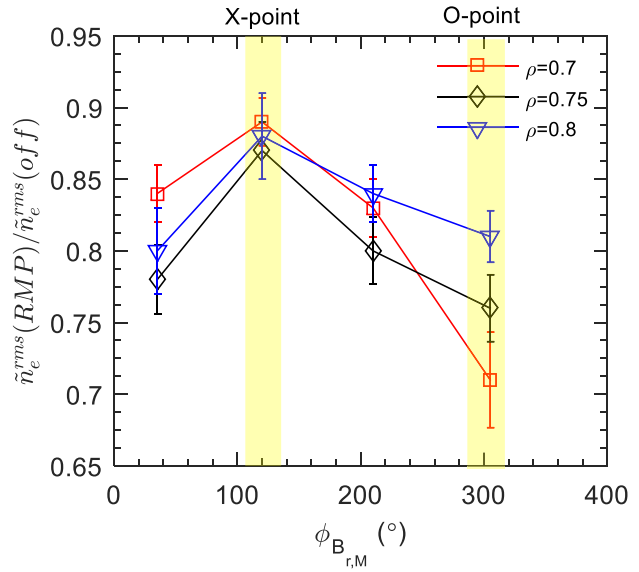

Figure 16. Relative density fluctuation level in term of four different toroidal RMP phases $\phi_{\mathrm{Br,M}}$ for different radial locations. The island center located at $\rho = 0.7$. Reproduced courtesy of IAEA. Figure from [55]. Copyright 2019 IAEA.

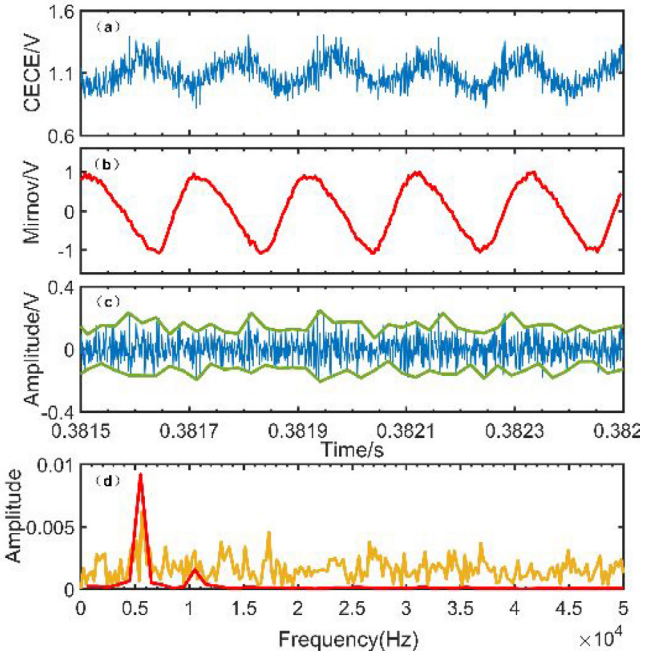

Figure 17. Impact of a rotating 2/1 island on the T_e fluctuations measured by CECE. (a) Original CECE signal, (b) Mirnov signal, (c) the CECE signal within 50–500 kHz (blue) and its envelop (green). The spectra are compared in (d) for the Mirnov signal (red), the positive envelop of (c) shown in yellow and the cross power spectrum of two band-pass filtered CECE signals near the $q = 2/1$ surface (blue). Reprinted from [56], with the permission of AIP Publishing.

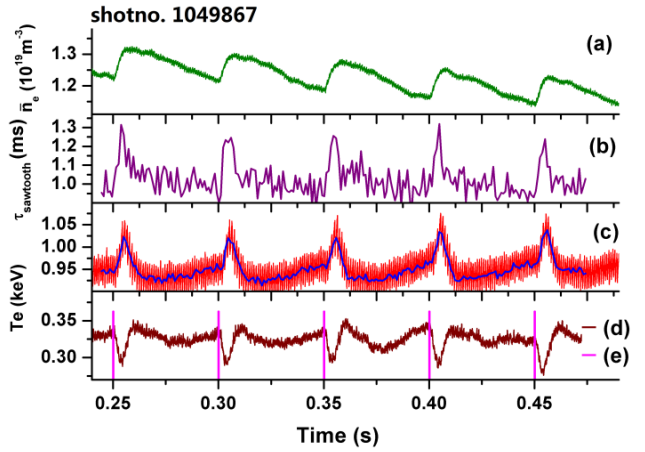

Figure 18. The waveforms of cold pulse discharge with multi-pulse SMBI; (a) line-averaged electron density, (b) sawtooth period, (c) core T_e, (d) edge T_e at $r/a = 0.79$, (e) SMBI pulse . Reproduced courtesy of IAEA. Figure from [57]. Copyright 2018 IAEA.

of the sign for the $m/n = 3/1$ electrostatic potentials appeared at $\Delta r = -1.5$ cm, where Δr is the distance from the last close flux surface (LCFS) with the minus sign representing inside the LCFS. The position of the $q = 3$ surface is indicated by the horizontal-dashed lines. The island width is evaluated as $w \sim \delta B_r^{0.5} \sim 1.5$ cm from the magnetic measurements. The X-points and O-points of the magnetic islands are identified from the sign of potential fluctuations, considering that the flows are toward the X-points. Based on the measurements of the $q = 3$ surface, island width and X-points, and assuming the 'separatrix' is satisfied with a sine or cosine function, the location of the magnetic islands is evaluated. The flows are concentrated near the separatrix and have quadrupole structures. The measurements are in good agreement with the prediction of theory [62]. The turbulence is concentrated near the X-points and partly trapped inside the islands (figure 15(b)).

The influence of the $m/n = 2/1$ magnetic island on density fluctuations [55] has been investigated by an eight-channel Doppler backscattering (DBS) reflectometer diagnostic [63]. The 2/1 islands were formed due to the penetration of the static RMP, and their phases with respect to the DBS measurement were scanned by varying the RMP phases between discharges.

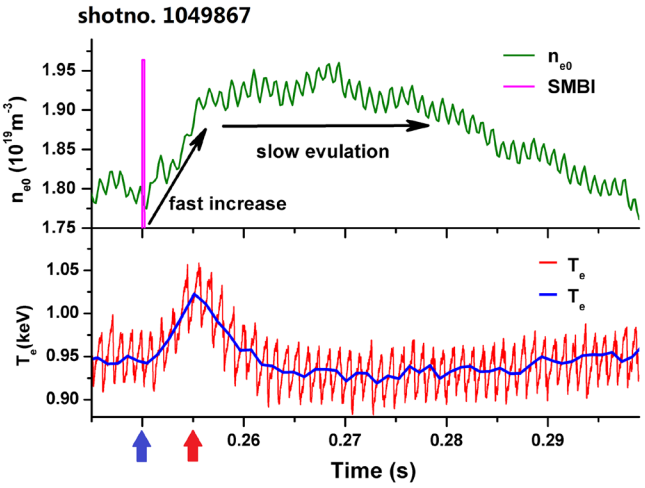

Figure 19. The detail time evolution of core n_e and T_e for the first SMBI pulse in figure 18. The blue line represents T_e at the middle time of each sawtooth cycle. Reproduced courtesy of IAEA. Figure from [57]. Copyright 2018 IAEA.

The island phases are indicated by the phase of $n = 1$ radial magnetic field, $\phi_{Br,M}$, measured by the locked mode detectors. It is found that density fluctuations reduced inside the island and elevated at the island boundary, as shown in figure 16, in agreement with the variations of temperature gradient induced by the magnetic island topology.

The influence of a rotating $m/n = 2/1$ magnetic island on the electron temperature fluctuations has been investigated by an eight-channel correlation ECE (CECE) diagnostic [56], as shown in figure 17. The 5 kHz rotating 2/1 island modulated both the original CECE signal, measured inside the island, and the Mirnov signals. Figure 17(*c*) shows the T_e fluctuations obtained by applying a band-pass filter (50–500 kHz) to the CECE signal. The envelope of the high frequency T_e fluctuations were also modulated by the rotation of the island, which can be observed more clearly in figure 17(*d*). The spectrum of Mirnov signal (red) shows a peak at 5 kHz due to the rotating island, while the 5 kHz peak in the spectrum of the positive envelope (yellow) reflects the modulation of island on turbulence. The cross-power spectrum of two band-pass filtered CECE signals near the $q = 2/1$ surfaces (blue) shows this clearer with reduced noise. The spatial structures of the n_e and T_e fluctuations around the 2/1 magnetic island are needed for further study and compared with that around the 3/1 edge island.

5.2. Observation of multi-channel non-local transport

The non-local transport (NLT) was triggered by applying multi-pulse SMBI as a cold pulse source in J-TEXT [57, 64]. In the recent cold pulse experiment, not only rapid electron temperature increases in the core are observed, but also steep rises in the inner density are found [57], as shown in figure 18. The typical NLT effect in electron channel (core T_e rises while edge T_e drops in figures 18(*c*) and (*d*)) appeared in all five SMBI pulses. On the other hand, the prompt increase of n_e due to SMBI is clearly shown in figure 18(*a*). Figure 19 displays more details for the particle transport during NLT from the local density response, where two different time scales of the core n_{e0} evolution appeared. One was the steep rise of n_{e0} in several milliseconds in the beginning. The other was the slow increase and sustainment in the following tens of milliseconds. Moreover, the steep rise of n_{e0} was synchronous with the fast increase of T_{e0}. For the J-TEXT SMBI experiments, the neutral penetration of SMBI mainly concentrated in plasma edge region ($r > 23$ cm). If the steep rise of n_{e0} was caused by local transport process, the averaged convection velocity from edge to core should be more than 40 m s^{-1} (~0.2 m/5 ms), which is astounding high value. The steep rise of n_{e0} should be also caused by some NLT process. One notable point during NLT is that the sawtooth period $\tau_{sawtooth}$ (figure 18(*b*)) also increased clearly for all five SMBI pulses. The increasing pace of $\tau_{sawtooth}$ was coincident with the core T_e rise. It is shown in [57] that the experimental Δn_e during NLT was much lower than the value needed to explain the prompt increase of $\tau_{sawtooth}$. An acceleration of core V_φ at around 1.4 km s^{-1} is estimated according to the scaling relation between V_φ and $\tau_{sawtooth}$. The J-TEXT results are the first experimental discovery of simultaneous fast NLT responses in multi-channels transport (electron temperature, particle, and momentum) in magnetic fusion plasma, and suggest that turbulence spreading [65, 66] is a possible mechanism for the NLT dynamics.

5.3. Theoretical study on the turbulence

Both the intrinsic rotation and the intrinsic current driven by micro-turbulence are important for magnetic confinement plasmas. However, the mechanisms for the origin of intrinsic rotation drive and intrinsic current drive are still open questions. We found a novel mechanism for the origin of intrinsic rotation driven by electrostatic ion temperature gradient (ITG) turbulence, which we refer to as turbulent acceleration [58, 59]. The turbulent acceleration cannot be written as a divergence of stress term, which is different from the physics of residual stress, and so acts as a local source or sink. In other words, the turbulent acceleration is an effective volume-force, while the divergence of residual stress is a kind of surface-force. We emphasize that the turbulent acceleration does not contradict momentum conservation law [60]. It is demonstrated that the conserved quantity corresponding to asymmetry of tokamak is the total canonical momentum or total momentum carried by both particles and electromagnetic fields but not the ion kinematic momentum or the ion flow velocity. The co-current turbulent acceleration driven by ITG turbulence vanishes for collisionless trapped electron mode (CTEM) turbulence [67], which may provide a possible theoretical explanation for the experimental observation of electron cyclotron heating (ECH) induced decrease of co-current core toroidal rotation in co-current neutral beam injection H-mode plasmas [68, 69]. Extension of our theory to electromagnetic (EM) ITG turbulence shows that the importance of electromagnetic effects to intrinsic parallel rotation drive [70].

Inspired by the investigation of intrinsic rotation driven by turbulence, we also present the intrinsic current (which is related to electron momentum) driven by EM electron

temperature gradient (ETG) turbulence [61]. There exist two types of intrinsic current driving mechanisms including the divergence of residual turbulent flux and the residual turbulent source. The local intrinsic current density driven by the residual turbulent flux for mesoscale variation of turbulent flux can reach about 80% of the bootstrap current density in the core region of an ITER standard scenario, but there is no net intrinsic current on a global scale. Thus, the q profile can be locally modified and the MHD could be affected. However, intrinsic current density driven by the residual turbulent source is small as compared with the bootstrap current and can be neglected.

The interplay between impurities and drift wave-zonal flow (ZF) system is systematically studied in the deuterium (D)–tritium (T) plasmas. The effects of various impurities on arbitrary radial wavelength residual ZF are investigated [71]. We found that even for the high ionized trace tungsten (W) with concentration being 10^{-4}, it can still significantly impact the level of residual ZF driven by trapped electron mode or ETG turbulence. The effects of helium ash from the D–T reaction on residual ZF depend on the temperature ratio between electron and impurity. The presence of impurity weakens the isotopic dependence of intermediate wavelength residual ZF. Meanwhile, it is shown that the normalized ZF growth rate driven by CTEM turbulence can be enhanced by fully ionized non-trace light impurities with relatively steep density profile [72]. Furthermore, we also found that the increase of hydrogenic ion mass could be favorable for the transport of fully ionized light impurity and high ionized W driven by ITG turbulence with relatively higher magnetic shear [73].

6. Summary and outlook

Over the last two years, the J-TEXT research has contributed to the impacts of 3D MP fields on magnetic topology, plasma disruptions, MHD instabilities, and plasma turbulence transport. The locked mode is avoided by the feedback application of RRMP and the TM can be suppressed by a negatively biased electrode. A new control strategy for TM control is proposed based on modulated static RMP and proved numerically. Further experimental research seems to be promising. The fluctuations of electron density, electron temperature, and plasma potential can be significantly modulated by the island structure. The RE generation and suppression has been studied, especially on their relationship with the magnetic perturbations. The MGI can cause MHD activities before disruptions, while the strong magnetic fluctuations during the CQ can suppress the RE generation. The RE generation can be actively suppressed by applying SMBI and RMP induced locked island. The SPI has been successfully applied to dissipate the MGI-induced runaway current for the first time on J-TEXT.

The TM control strategies proposed and tested on J-TEXT reveal the important role of plasma rotation. By applying either rotating/pulsed RMP field or electrode biasing, the plasma rotation is accelerated, the TM is then suppressed and the LM can be avoided. Although these strategies might face engineering difficulties with application to ITER or a fusion reactor, the related mechanisms might be helpful for understanding the fusion plasmas and hence developing an alternative control strategy for TM and disruption, because the plasma rotation is predicted to be low in ITER and hence the locked mode tends to appear.

The success of RE suppression via RMP might be applicable for ITER or fusion reactor. The required 2/1 locked island can be easily formed by using the static $n = 1$ RMP field, which should be available via the error field correction coils installed outside the blanket. Further validation on the physical feasibility of RMP controlling REs is needed in a larger machine. The injection of a large amount of impurity by SPI is more prospective than MGI for the safe operation of ITER due to its deeper penetration and higher mixing efficiency. However, the delay times from SPI trigger to the mitigated thermal quench on ITER might be more than 30 ms [37] with the pellet velocity of ~150 m s^{-1}, hence a reliable disruption prediction system is needed with sufficient warning time. The recent research on the prediction for density limit disruptions will be further extended to more types of disruptions, such as the locked mode disruptions, on J-TEXT.

In the following two years, several new diagnostics and auxiliary systems will be available on J-TEXT. The ECE-imaging, VUV spectrometer, and Doppler reflectometry can provide more information for the study of MHD activities, turbulence and transport. The divertor configuration will be tested using the high-field X-point configuration and the island divertor concept [74], respectively. The 105 GHz/0.5 MW/1 s ECRH system will be commissioned in 2019 [75]. It will support the plasma heating, current drive and hence disruption and MHD instability control.

Acknowledgments

This work is supported by the National Magnetic Confinement Fusion Science Program of China (Nos. 2015GB111001, 2015GB111002, 2015GB120003 and 2014GB118000) and the National Natural Science Foundation of China (Nos. 11505069, 11575067, 11405068 and 11275079).

Appendix. The J-TEXT Team

Yunfeng Liang[1,2,3], Yuan Pan[1], Kenneth William Gentle[4], Xiwei Hu[1], Kexun Yu[1], Qingquan Yu[5], Ge Zhuang[1,6], Yonghua Ding[1], Ming Zhang[1], Li Gao[1], Lu Wang[1], Zhongyong Chen[1], Zhijiang Wang[1], Zhonghe Jiang[1], Zhipeng Chen[1], Zhoujun Yang[1], Zhifeng Cheng[1], Xiaoqing Zhang[1], Minghai Liu[1], Tao Xu[1], Wei Jiang[7], Lin Yi[7], Yanli Peng[7], Ya Zhang[8], Bo Rao[1], Qiming Hu[9], Donghui Xia[1], Wei Zheng[1], Shaoxiang Ma[1], Yong Yang[1], Chuan Li[1], Nengchao Wang[1], Peng Shi[1], Jianchao Li[10], Xiaolong Zhang[10], Hai Liu[11], Wei Yan[1], Weixin Guo[1], Weijun Wang[1], Mei He[1], Qing Zhao[1], Jiayu Xu[1], Gangyi Zhou[1], Cheng Yang[1], Renjie Guo[1], Junjie Yao[1], Chuliang Wang[1], Weigang Ba[1], Jingwei Fu[1], Meiling Liang[1], Yehong Guan[1], Bin Peng[1], Hongyan Wu[1], Long Zeng[3], Huaxiang

Zhang[3], Kaijun Zhao[12], Wulyu Zhong[13], Min Jiang[13], Yunbo Dong[13], Min Xu[13], Aike Wang[13], Jun Cheng[13], Lin Nie[13], Rui Ke[13], Jianqiang Xu[13], Zengchen Yang[13], Jie Wen[13], Peiwan Shi[13], Anshu Liang[13], Yipo Zhang[13], Yifan Wu[13], Chengyuan Chen[13], Yuejiang Shi[14], SeongMoo Yang[14], He Huang[4], William L. Rowan[4], Max Austin[4], Sanggon Lee[15], Neville C. Luhmann Jr.[16], Calvin W. Domier[16], Yilun Zhu[16], Weixing Ding[17], David L. Brower[18], J. Chen[18], Yue Dai[1], Fuming Li[1], Guozhong Jiang[1], Jun Zhang[1], Guozhen Zheng[1], Chao Yang[1], Lizhi Zhu[1], Xiaoming Pan[1], Jiyang He[1], Changhai Liu[1], Zhong Zeng[1], Yiren Zhu[1], Mingxiang Huang[1], Shuitao Peng[1], Xiang Jian[1], Qiang Liu[1], Feiran Hu[1], Linzi Liu[1], Ruihai Tong[1], Zhengqing Zhang[1], Shucai Li[1], Xiao Liang[1], Hao Cai[1], Chi Zhang[1], Jin Jiao[1], Tiankui Ma[1], Ruobing Zhou[1], Xuan Li[1], Junren Wang[1], Panfeng Zheng[1], Jun Shao[1], Linglong Li[1], Kuanhong Wan[1], Zhenxiong Yu[1], Jia Liu[1], Minxiong Yan[1], Fangtai Cui[1], Jian Lv[1], Xinke Ji[1], Haiyan Ma[1], Haohui Xu[1], Zongchang Sun[1], Yang Li[1], Qingshuang Qiu[1], Guo Xu[1], Shuangyun Zhao[1], Yuan Li[1], Bicheng Li[1], Xueling Wang[1], Siquan Li[1], Anjue Dai[1], Jiefeng Huang[1], Hailong Gao[1], Bowen Ruan[1], Daojing Guo[1], Wen He[1], Yunong Wei[1], Yinan Zhou[1], Da Li[1], Mao Li[1], Zhuo Huang[1], Zhifang Lin[1], Ruo Jia[1], Xueliang Zhang[1], Nianheng Cai[1],Xianli Xie[1], Chengxi Zhou[1], Ying He[1], Yue Peng[1], Qi Zhang[1], Hanhui Li[1], Pengyu Wang[1], Xin Xu[1], Song Zhou[1], Dongyu Wang[1], Jiawei Li[1], Tingting Yang[1], Conghui Lu[1], Jie Yang[1], Minghui Xia[1], You Li[1], Huaiyu Yang[1], Jing Huang[1], Lai Peng[1], Zebao Song[1], Ming Chen[1], Xueqing Zhao[1], Yikun Jin[1], Junli Zhang[1], Qinxue Cai[1], Hao Zhou[1], Xiao Ma[1], Rumeng Wang[1], Jingjun Zhou[1], Weiwei Zhang[1], Xiaoyi Zhang[1], Mingcong Zhu[1], Haisen Mo[1], Liuxiu He[1], Zhou Yang[1], Huapu Deng[1], Jie Hu[1], Duoqin Wang[1], Wei Li[1], Zichao Xu[1], Wei Zhang[1], Chengshuo Shen[1], Xin Ye[1], Changhong Li[1], Yuxing Wang[1], Yiwei Lu[1], Lan Zhou[1], Jiapeng Xiao[1], Yixiong Zhang[1], Yizhe Tian[1], Aoxiang Wang[1], Haotian Huang[1], Fengqi Chang[1], Jing Zhou[1], Jingjing Xuan[1], Zhi Liu[1], Chengjin Qian[1], Tong Wang[1], Yuan Huang[1], Zheng Zhou[1], Zhigang Hao[1], Qiong Li[1], Jinyu Xiong[1], Huakun Cai[1], Mingzhu Zhang[1], Yaping Zhang[1], Haotian Liang[1], Yangming Zhao[1], Qiancheng Zhao[1], Wei Bai[1], Yu Zhong[1], Shaodong Jiao[1], Dongliang Han[1], Shiyi Peng[1], Jiaolong Dong[1], Qinglong Yang[1], Fan Gu[1], Zhaosu Wang[1], Hao Wang[1], Shu Yang[1], Yang Zhao[1], Wang Lin[1], Zhe Liu[1], Guoyao Fan[1], Kehong Dong[1], Guodong Zhang[1], Xixuan Chen[1], Xiehang Ren[1], Feng Li[1], Ce Deng[1], Feng Han[1], Jing Liu[1], Qiqi Wu[1] and Fei Xie[1]

[1]International Joint Research Laboratory of Magnetic Confinement Fusion and Plasma Physics, State Key Laboratory of Advanced Electromagnetic Engineering and Technology, School of Electrical and Electronic Engineering, Huazhong University of Science and Technology, Wuhan 430074, People's Republic of China

[2]Forschungszentrum Jülich GmbH, Institut für Energie- und Klimaforschung—Plasmaphysik, 52425 Jülich, Germany

[3]Institute of Plasma Physics, Chinese Academy of Sciences, Hefei 230031, People's Republic of China

[4]University of Texas, Austin, TX 78712, United States of America

[5]Max-Planck-Institut für Plasmaphysik, D-85748 Garching, Germany

[6]University of Science and Technology of China, Hefei 230026, People's Republic of China

[7]School of Physics, Huazhong University of Science and Technology, Wuhan 430074, People's Republic of China

[8]Department of Physics, Wuhan University of Technology, Wuhan 430070, China

[9]Princeton Plasma Physics Laboratory, PO Box 451, Princeton, NJ 08543, United States of America

[10]Advanced Energy Research Center, Shenzhen University, Shenzhen 518060, People's Republic of China

[11]Southwest Jiaotong University, Chengdu, People's Republic of China

[12]College of Nuclear Science and Engineer, East China University of Technology, PO Box 330013, Nanchang, China

[13]Southwestern Institute of Physics, Chengdu 610041, People's Republic of China

[14]Department of Nuclear Engineering, Seoul National University, Seoul, Korea, Republic of

[15]National Fusion Research Institute, Daejeon 305-333, Korea, Republic of

[16]University of California, Davis, CA 95616, United States of America

[17]University of Wisconsin—Madison, 53706 Madison, WI, United States of America

[18]University of California Los Angeles, Los Angeles, CA 90095, United States of America

ORCID iDs

N.C. Wang https://orcid.org/0000-0001-6797-2398
Z.Y. Chen https://orcid.org/0000-0002-8934-0364
Z.P. Chen https://orcid.org/0000-0002-8330-0070
Q.M. Hu https://orcid.org/0000-0002-8877-4988
Z.F. Cheng https://orcid.org/0000-0001-6019-399X
L. Wang https://orcid.org/0000-0002-5881-6139
Z.H. Jiang https://orcid.org/0000-0002-4971-080X
L. Zeng https://orcid.org/0000-0003-4968-1401
Y.J. Shi https://orcid.org/0000-0002-9572-3310
W.X. Guo https://orcid.org/0000-0001-7677-799X
M. Zhang https://orcid.org/0000-0002-9372-4926

References

[1] Zhuang G. *et al* 2011 *Nucl. Fusion* **51** 094020
[2] Zhuang G. *et al* 2013 *Nucl. Fusion* **53** 104014
[3] Zhuang G. *et al* 2015 *Nucl. Fusion* **55** 104003
[4] Zhuang G. *et al* 2017 *Nucl. Fusion* **57** 102003
[5] Ding Y.H. *et al* 2018 *Plasma Sci. Technol.* **20** 125101
[6] Ikeda K. 2007 *Nucl. Fusion* **47**
[7] Wan Y.X. *et al* 2017 *Nucl. Fusion* **57** 102009
[8] Rao B. *et al* 2013 *Fusion Eng. Des.* **89** 378
[9] Huang Z. *et al* 2017 Non monotonic dependence of the 2/1 RMP field penetration threshold on density in J-TEXT *643rd WEH Seminar Impact of 3D Magnetic Fields on Hot Plasmas (Bad Honnef, Germany, 22–24 May 2017)*
[10] Li Y. *et al* 2018 *Rev. Sci. Instrum.* **89** 10K116
[11] Hender T.C. *et al* 2007 Progress in the ITER Physics Basis Chapter 3: MHD stability, operational limits and disruptions *Nucl. Fusion* **47** S128

[12] de Vries P.C. *et al* 2011 *Nucl. Fusion* **51** 053018
[13] Sweeney R. *et al* 2017 *Nucl. Fusion* **57** 016019
[14] Fitzpatrick R. 1993 *Nucl. Fusion* **33** 1049
[15] Hu Q. *et al* 2013 *Phys. Plasmas* **20** 092502
[16] Rao B. *et al* 2013 *Phys. Lett.* A **377** 315
[17] Li D. *et al* 2018 Recent progresses on the RMP researches towards active control of tearing mode in the J-TEXT tokamak *Preprint: 2018 IAEA Fusion Energy Conf. (Gandhinagar, India, 22–27 October 2018)* EX/P3-13
[18] Hender T.C. *et al* 1992 *Nucl. Fusion* **32** 2091
[19] Rao B. *et al* 2013 *Plasma Phys. Control. Fusion* **55** 122001
[20] Hu Q.M. *et al* 2014 *Nucl. Fusion* **54** 122006
[21] Hu Q.M. *et al* 2014 *Nucl. Fusion* **54** 064013
[22] Cheng Z.F. *et al* 2013 *Rev. Sci. Instrum.* **84** 073508
[23] Jin W. *et al* 2012 *Rev. Sci. Instrum.* **83** 10E502
[24] Jin W. *et al* 2014 *Rev. Sci. Instrum* **85** 023509
[25] Yan W. *et al* 2018 *Plasma Phys. Control. Fusion* **60** 035007
[26] Xu G. *et al* 2018 *Plasma Sci. Technol.* **20** 085601
[27] Li M. *et al* 2019 *Fusion Eng. Des.* accepted (https://doi.org/10.1016/j.fusengdes.2019.03.122)
[28] Jin H. *et al* 2015 *Plasma Phys. Control. Fusion* **57** 104007
[29] Wang N.C. *et al* 2019 *Nucl. Fusion* **59** 026010
[30] Hu Q. and Yu Q. 2016 *Nucl. Fusion* **56** 034001
[31] Yan M.X. *et al* 2017 *Fusion Eng. Des.* **115** 17
[32] Zheng W. *et al* 2018 *IEEE Trans. Nucl. Sci.* **65** 2344
[33] Rao B. *et al* 2016 *Rev. Sci. Instrum.* **87** 11D425
[34] Liu H. *et al* 2017 *Nucl. Fusion* **57** 016003
[35] Hollmann E.M. *et al* 2015 *Phys. Plasmas* **22** 021802
[36] Reux C. *et al* 2015 *Nucl. Fusion* **55** 093013
[37] Lehnen M. *et al* 2018 R&D for reliable disruption mitigation in ITER *Preprint: 2018 IAEA Fusion Energy Conf. (Gandhinagar, India, 22–27 October 2018)* EX/P7-12
[38] Zeng L. *et al* 2017 *Nucl. Fusion* **57** 046001
[39] Li S.C. *et al* 2017 *Plasma Phys. Control. Fusion* **59** 055003
[40] Chen Z.Y. *et al* 2016 *Nucl. Fusion* **56** 074001
[41] Chen Z.Y. *et al* 2018 *Nucl. Fusion* **58** 082002
[42] Lin Z.F. *et al* 2019 *Plasma Phys. Control. Fusion* **61** 024005
[43] Huang D.W. *et al* 2017 *Plasma Phys. Control. Fusion* **59** 085002
[44] Zeng L. *et al* 2013 *Phys. Rev. Lett.* **110** 235003
[45] Helander P. *et al* 2004 *Phys. Plasmas* **11** 5704
[46] Zeng L. *et al* 2015 *J. Plasma Phys.* **81** 475810402
[47] Huang Y. *et al* 2018 *Nucl. Fusion* **58** 126024
[48] Xiao J.S. *et al* 2014 *Plasma Sci. Technol.* **16** 17
[49] Abdullaev S.S. *et al* 2015 *Phys. Plasmas* **22** 040704
[50] Ding Y.H. *et al* 2013 *Plasma Sci. Technol.* **15** 1154
[51] Wang S.Y. *et al* 2016 *Plasma Phys. Control. Fusion* **58** 055014
[52] Zheng W. *et al* 2018 *Nucl. Fusion* **58** 056016
[53] Zheng W. *et al* 2018 *IEEE Trans. Nucl. Sci.* **65** 771
[54] Zhao K.J. *et al* 2017 *Nucl. Fusion* **57** 126006
[55] Jiang M. *et al* 2019 *Nucl. Fusion* **59** 046003
[56] Zhou H. *et al* 2018 *Rev. Sci. Instrum.* **89** 10H105
[57] Shi Y.J. *et al* 2018 *Nucl. Fusion* **58** 044002
[58] Wang L. *et al* 2018 Theory of turbulence driven intrinsic rotation and current *Preprint: 2018 IAEA Fusion Energy Conf. (Gandhinagar, India, 22–27 October 2018)* TH/P6-4
[59] Wang L. and Diamond P.H. 2013 *Phys. Rev. Lett.* **110** 265006
[60] Peng S.T. and Wang L. 2017 *Phys. Plasmas* **24** 012304
[61] He W. *et al* 2018 *Nucl. Fusion* **58** 106004
[62] Biskamp D. 2000 *Magnetic Reconnection in Plasmas* (Cambridge: Cambridge University Press)
[63] Shi Z.B. *et al* 2016 *Rev. Sci. Instrum.* **87** 113501
[64] Xiao J.S. *et al* 2013 *IEEE Trans. Plasma Sci.* **41** 3675
[65] Garbet X. *et al* 1994 *Nucl. Fusion* **34** 963
[66] Diamond P.H. *et al* 1995 *Phys. Plasmas* **2** 3640
[67] Wang L. *et al* 2016 *Phys. Plasmas* **23** 042309
[68] Shi Y.J. *et al* 2013 *Nucl. Fusion* **53** 113031
[69] McDermott R.M. *et al* 2011 *Plasma Phys. Control. Fusion* **53** 124013
[70] Peng S.T. *et al* 2017 *Nucl. Fusion* **57** 036003
[71] Guo W.X. *et al* 2017 *Nucl. Fusion* **57** 126052
[72] Guo W.X. *et al* 2017 *Nucl. Fusion* **57** 056012
[73] Guo W.X. *et al* 2016 *Phys. Plasmas* **23** 112301
[74] Zhou S. *et al* 2019 *Fusion Eng. Des.* accepted (https://doi.org/10.1016/j.fusengdes.2019.01.109)
[75] Xia D.H. *et al* 2019 *EPJ Web Conf.* **203** 04017